

## Economic assessment of greenhouse gas reduction through low-grade waste heat recovery using organic Rankine cycle (ORC)<sup>†</sup>

Muhammad Imran<sup>1,2</sup>, Byung-Sik Park<sup>1,2,\*</sup>, Hyouck-Ju Kim<sup>1,2</sup>, Dong-Hyun Lee<sup>2</sup> and Muhammad Usman<sup>1,2</sup>

<sup>1</sup>Energy System Engineering, University of Science & Technology, Daejeon, 305–350, Korea

<sup>2</sup>Energy Network Team, Korea Institute of Energy Research, Daejeon, 305–343, Korea

(Manuscript Received May 25, 2014; Revised September 16, 2014; Accepted October 25, 2014)

### Abstract

Low-grade waste heat recovery technologies reduce the environmental impact of fossil fuels and improve overall efficiency. This paper presents the economic assessment of greenhouse gas (GHG) reduction through waste heat recovery using organic Rankine cycle (ORC). The ORC engine is one of the mature low temperature heat engines. The low boiling temperature of organic working fluid enables ORC to recover low-temperature waste heat. The recovered waste heat is utilized to produce electricity and hot water. The GHG emissions for equivalent power and hot water from three fossil fuels—coal, natural gas, and diesel oil—are estimated using the fuel analysis approach and corresponding emission factors. The relative decrease in GHG emission is calculated using fossil fuels as the base case. The total cost of the ORC system is used to analyze the GHG reduction cost for each of the considered fossil fuels. A sensitivity analysis is also conducted to investigate the effect of the key parameter of the ORC system on the cost of GHG reduction. Throughout the 20-year life cycle of the ORC plant, the GHG reduction cost for R245fa is 0.02 \$/kg to 0.04 \$/kg and that for pentane is 0.04 \$/kg to 0.05 \$/kg. The working fluid, evaporation pressure, and pinch point temperature difference considerably affect the GHG emission.

**Keywords:** Economic assessment; Greenhouse gas; Organic rankine cycle; Waste heat recovery

### 1. Introduction

The leftover heat produced by combustion or any chemical or thermal process is known as waste heat because it is usually exhausted directly to the environment. Waste heat has not only the highest value of exergy but also a high concentration of pollutants, including carbon dioxide (CO<sub>2</sub>), nitrogen oxides (NO<sub>x</sub>), and sulfur oxides (SO<sub>x</sub>), which are responsible for global warming [1]. Electricity, heat generation, and transportation account for two-thirds of the global CO<sub>2</sub> emission [2]. The large concentrations of CO<sub>2</sub> in these two sectors can be attributed to the usage of fossil fuels coal, natural gas, and petroleum. The CO<sub>2</sub> emission from each sector is shown in Fig. 1. The amount of the waste heat from industrial processes accounts for 20% to 50% of the input heat, and the recovery of this heat can improve energy efficiency by 10% to 50% [3]. About 50% of industrial waste heat has a low temperature ranging from 100°C to 120°C [4].

Moreover, waste heat recovery reduces the environmental impact by limiting the use of fossil fuels [5]. The key factors that determine the feasibility of waste heat recovery include

■ Residential ■ Other ■ Industry ■ Transport ■ Electricity & Heat

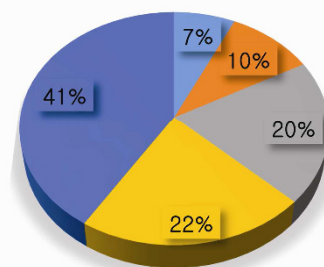


Fig. 1. World CO<sub>2</sub> emission for each sector in 2010 [2].

flow rate, temperature, pressure, chemical composition, allowable temperature and pressure drop, operating schedules, availability, and other logistics of heat source.

The selection of appropriate waste heat recovery system directly effects the efficiency and cost. The waste heat source characteristics and appropriate waste heat recovery technologies are shown in Table 1.

Combined heat and power (CHP) systems and tri-generation systems (TGS) provide a sustainable path toward reducing greenhouse gas (GHG) emission and dependency on fossil fuels. CHP systems are suitable for the simultaneous production of heat and power, whereas TGS are used for the

\*Corresponding author. Tel.: +82 42 8653323, Fax.: +82 42 8653756

E-mail address: bspark@kier.re.kr

<sup>†</sup>Recommended by Associate Editor Tong Seop Kim

© KSME & Springer 2015

Table 1. Waste heat source and corresponding heat recovery technologies [3].

Temperature	Heat sources	Temperature (°C)	Heat recovery methods
High temperature [> 650°C]	Nickel refining furnace	1370 to 1650	<ul style="list-style-type: none"> <li>· Combustion air preheat</li> <li>· Steam generation for process heating or for mechanical/electrical work</li> <li>· Furnace load preheating</li> <li>· Transfer to medium to low-temperature processes</li> </ul>
	Steel electric arc furnace	1370 to 1650	
	Basic oxygen furnace	1200 to 1250	
	Aluminum reverberatory furnace	1100 to 1200	
	Copper refining furnace	760 to 820	
	Steel heating furnace	930 to 1040	
	Copper reverberatory furnace	900 to 1090	
	Hydrogen plants	650 to 980	
	Fume incinerators	650 to 1430	
	Glass melting furnace	1300 to 1540	
	Coke oven	650 to 1000	
	Iron cupola	820 to 980	
Medium temperature [230°C to 650°C]	Steam boiler exhaust	230 to 480	<ul style="list-style-type: none"> <li>· Combustion air preheating</li> <li>· Steam/ power generation</li> <li>· ORC</li> <li>· Furnace load preheating</li> <li>· Feed water preheating</li> </ul>
	Gas turbine exhaust	370 to 540	
	Reciprocating engine exhaust	320 to 590	
	Heat treating furnace	430 to 650	
	Drying and baking ovens	230 to 590	
	Cement kiln	450 to 620	
Low temperature [< 230°C]	Exhaust gases exiting recovery devices in gas fired boilers, ethylene furnaces, and so on	70 to 230	<ul style="list-style-type: none"> <li>· Space heating</li> <li>· Domestic water heating Upgrading via a heat pump to increase temp for end use</li> <li>· ORC</li> <li>· Kalina Cycle</li> </ul>
	Process steam condensate cooling water from		
	Furnace doors	30 to 50	
	Annealing furnaces	70 to 250	
	Air compressors	30 to 50	
	Internal combustion engines	70 to 120	
	Air conditioning and refrigeration condensers	30 to 40	
	Drying, baking, and curing ovens	90 to 230	
Hot processed liquids/solids	30 to 230		

simultaneous production of heating, cooling, and power [6]. The recovery of waste heat through CHP and TGS can increase the system exergy efficiency up to 70% [7, 8]. The economic aspect and feasibility of waste heat recovery-based CHP system and TGS have been analyzed in terms of their thermodynamic performance [9, 10]. The GHG emission and exergo-environmental analysis of TGS was presented by Ref. [11]. The comparison of the results with those of the conventional CHP system shows that the exergy efficiency of TGS is higher but its environmental effect is lower. The exergo-environmental optimization of a gas turbine-based CHP system was performed by Ref. [12] using a genetic algorithm. A sensitivity analysis was conducted at various power levels of the gas turbine and shows a decrease in the specific unit cost of fuel with an increase in net power.

The economic feasibility of the GHG reduction potential of low-grade waste heat recovery through the organic Rankine cycle (ORC) has not yet been reported in the literature. The current study investigates the GHG reduction potential of the ORC waste heat recovery system. The study

also provides an economic assessment and examines the effect of the operating parameters of ORC on the economics of GHG reduction.

## 2. System description

The current system has three sections: the heat source, ORC, and hot water. The schematic of the system is shown in Fig. 2.

The heat source is from a kiln with a constant flow rate and temperature recovered from the heat recovery vapor generator (HRVG).

The ORC has four main components: the HRVG, expander, condenser, and pump. An organic fluid with a low boiling point recovers the heat from the heat source in HRVG and vaporizes it. High-pressure vapors expand through the turbine to produce power. The vapors are condensed in the condenser and pumped back to the HRVG, after which the cycle is repeated. The hot water produced by the condenser has a temperature of about 45°C to 50°C, which is suitable for household applications.

Table 2. Heat source conditions.

Factor	Value
Heat source	Exhaust (51.2% CO <sub>2</sub> , 48.8% N <sub>2</sub> )
Conditions	T= 180°C and $\dot{m} = 10 \text{ kg/s}$

Table 3. Operating conditions of the ORC system.

Factor	Value
Isentropic efficiency of turbine	0.85
Isentropic efficiency of pump	0.75
Superheat at turbine inlet	2 °C
Evaporation pressure	5–20 bar
Pinch point temperature in evaporator	10°C

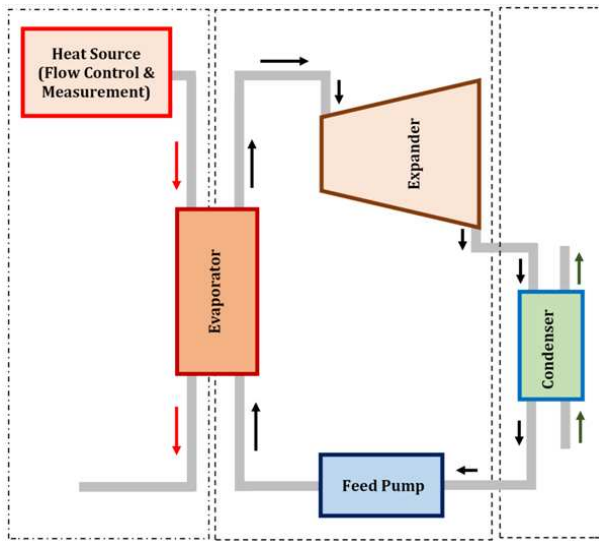


Fig. 2. Schematic of the ORC waste heat recovery system.

### 3. Modeling

The constant temperature heat source was considered, and the particulars of the heat source are shown in Table 2.

The heat source was utilized to produce power during the expansion in the turbine and hot water during the condensation of the working fluid in the condenser. The evaporation pressure of the working fluid varied from 5 bar to 20 bar, and the corresponding net power and hot water capacity were calculated. The operating pressure and pinch point in the evaporator were varied and optimized because of their strong influence on the ORC performance. The operating parameters of the ORC system are shown in Table 3.

The following assumptions were taken in modeling the ORC system:

- The ORC system operates at steady state conditions.
- The thermal and friction losses in the pipes are negligible.
- The pump and turbine models are based on constant isentropic efficiency.
- The heat loss from the ORC components is negligible.

Two working fluids—R245fa and pentane—were selected for the ORC system. The emission of these two working fluids was estimated using the lifecycle assessment of the ORC power plant during operation [13].

The lifecycle of the ORC power plant was divided into construction, operation, and decommissioning phases. The current study includes only the environmental impact of R245fa and pentane during the operation phase. The GHG emission is low because of the lack of combustion in ORC.

For the economic assessment, a module costing technique was used to calculate the individual cost of the ORC components [14, 15]. In the module costing technique, the component cost was based on the key parameters of that component (e.g., area in the case of heat exchangers), and the proper indexes were used to include the effect of size, material, key parameters, and time.

In the next step, the GHG emission from fossil fuel power plants (coal, natural gas, and diesel) was estimated for equivalent electricity and hot water to the ORC system. The GHG emission from the ORC plant were subtracted from the GHG emission of the fossil fuels to analyze the reduction of GHG emission. The cost of GHG emission was calculated by dividing the GHG reduction by the total cost of the ORC system.

#### 3.1 Turbine and pump model

The turbine and pump are modeled after their isentropic efficiency. For the pump,

$$\eta_{isen} = \frac{h_{out,s} - h_{in}}{h_{out} - h_{in}} \quad (1)$$

For turbine,

$$\eta_{isen} = \frac{h_{in} - h_{out}}{h_{in} - h_{out,s}} \quad (2)$$

#### 3.2 Evaporator and condenser model

The evaporator and condenser have a plate-type heat exchanger and are divided into three sections: single phase (liquid), two phase, and single phase (vapors). The design is based on the LMTD method, and the iterative process of the design is shown in Fig. 3.

##### 3.2.1 Single phase design of the evaporator and condenser

The overall heat transfer coefficient of the single phase is calculated as follows:

$$\frac{1}{U_{sp}} = \frac{1}{\alpha_w} + \frac{t_p}{k_p} + \frac{1}{\alpha_{r,sp}} \quad (3)$$

The single phase Nusselt No. correlation for the heat source in the plate heat exchanger [16] can be obtained as follows:

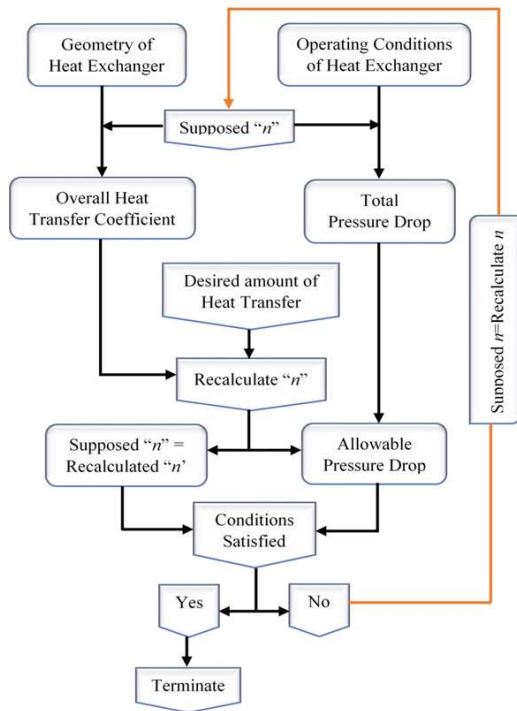


Fig. 3. Design layout of the heat evaporator and condenser.

$$Nu_w = 0.724 \left( \frac{6\beta}{\pi} \right)^{0.646} Re^{0.583} Pr^{0.33} \tag{4}$$

The single phase Nusselt No. correlation for R245fa in the plate heat exchanger [17] can be obtained by the following equation:

$$\alpha_{r,sp} = 0.2092 \left( \frac{k_f}{D_h} \right) Re^{0.78} Pr^{0.33} \left( \frac{\mu_m}{\mu_{wall}} \right)^{0.14} \tag{5}$$

The pressure drop in the single phase for both cold and hot side fluids consists of only the frictional pressure drop. The pressure drop caused by the elevation and the port pressure loss are neglected in the single phase.

$$\Delta P = \frac{4fNcG^2L}{2\rho D_h} \tag{6}$$

The single phase frictional pressure drop factor for both cold and hot sides [16] are obtained as follows:

$$f = \frac{C}{Re^p} \tag{7}$$

**3.2.2 Two-phase design of the evaporator and condenser**

The two-phase overall heat transfer coefficient can be obtained as follows:

$$\frac{1}{U_{tp}} = \frac{1}{\alpha_w} + \frac{t_p}{k_p} + \frac{1}{\alpha_r} \tag{8}$$

The Nusselt No. correlation for the R245fa evaporation in the plate heat exchanger [18] can be calculated as follows:

$$Nu = Ge_1 Re_{eq}^{Ge_2} Bo_{eq}^{0.3} Pr^{0.4} \tag{9}$$

where

$$Ge_1 = 2.81 \left( \frac{P_{co}}{D_h} \right)^{-0.041} \left( \frac{\pi}{2} - \beta \right)^{-2.83} \tag{10}$$

$$Ge_2 = 2.81 \left( \frac{P_{co}}{D_h} \right)^{-0.082} \left( \frac{\pi}{2} - \beta \right)^{0.61}$$

The equivalent Reynolds number and boiling number are given by the following:

$$Re_{eq} = \frac{GeqD_h}{\mu_f} \quad ; \quad Bo_{eq} = \frac{q''}{Geq \times i_{fg}} \tag{11}$$

$$eq = G \left[ (1-x) + x \left( \frac{\rho_f}{\rho_g} \right)^{0.5} \right]$$

The two-phase friction factor [18] is obtained as follows:

$$f = Ge_3 Re_{eq}^{Ge_4} \tag{12}$$

where

$$Ge_3 = 64710 \left( \frac{P_{co}}{D_h} \right)^{-5.27} \left( \frac{\pi}{2} - \beta \right)^{-3.03} \tag{13}$$

$$Ge_4 = -1.314 \left( \frac{P_{co}}{D_h} \right)^{-0.62} \left( \frac{\pi}{2} - \beta \right)^{-0.47}$$

For the R245fa condensation in the plate heat exchanger [19],

$$Nu = Ge_5 Re_{eq}^{Ge_6} Bo_{eq}^{0.3} Pr^{0.4} \tag{14}$$

where

$$Ge_5 = 11.22 \left( \frac{P_{co}}{D_h} \right)^{-0.041} \left( \frac{\pi}{2} - \beta \right)^{-4.5} \tag{15}$$

$$Ge_6 = 0.35 \left( \frac{P_{co}}{D_h} \right)^{0.23} \left( \frac{\pi}{2} - \beta \right)^{1.48}$$

The two-phase frictional factor for the condensation pressure drop [19] is calculated as follows:

$$f = Ge_3 Re_{eq}^{Ge_4}, \tag{16}$$

where

$$Ge_7 = 3521.1 \left( \frac{P_{co}}{D_h} \right)^{4.17} \left( \frac{\pi}{2} - \beta \right)^{-7.75} \tag{17}$$

$$Ge_8 = -1.024 \left( \frac{P_{co}}{D_h} \right)^{0.0925} \left( \frac{\pi}{2} - \beta \right)^{-1.3}.$$

The heat transfer coefficient of the water side [16] is computed as follows:

$$Nu_w = 0.724 \left( \frac{6\beta}{\pi} \right)^{0.646} Re^{0.583} Pr^{0.33}. \tag{18}$$

The pressure drop in the two phase consists of the pressure drop caused by the acceleration of the refrigerant, change in elevation, inlet/exit manifolds, and friction inside the corrugated plate heat exchanger. The frictional pressure drop inside the plate heat exchanger is calculated as follows:

$$\Delta P_f = \frac{4fNcG^2L}{2\rho D_h}. \tag{19}$$

The pressure drop caused by acceleration is represented by the following:

$$\Delta P_{ac} = G_r^2 \times x \times (v_g - v_f), \tag{20}$$

where  $G_r$  is the channel flow area

$$G_r = \frac{m_r}{b \times Nc \times W_p}. \tag{21}$$

The change in the pressure caused by the elevation is calculated as follows:

$$\Delta P_{elev} = g \times \rho_m \times L_e. \tag{22}$$

The port pressure drop can be obtained as follows:

$$\Delta P_{port} = \frac{1.5 \times G_r^2 \times v_m}{2}. \tag{23}$$

### 3.3 Economic modeling

The maintenance cost is not included in the economic modeling. The cost of individual components is calculated using the appropriate chemical engineering plant cost index for 2013. The cost of the evaporator and condenser are given as

$$C_{HX} = \frac{527.7}{397} F_S \dot{C}_{HX} \left\{ B_{1,HX} + (B_{2,HX} F_{M,HX} F_{P,HX}) \right\}, \tag{24}$$

where  $F_S$  is an additional factor for the overhead cost,  $B_{1,HX}$  and  $B_{2,HX}$  are constants for the heat exchanger type, and  $F_{M,HX}$  is the additional material factor for the heat exchanger. The  $F_{P,HX}$  is the pressure factor for the heat exchanger, and  $\dot{C}_{HX}$  is the basic cost of the heat exchanger made from stainless steel. The basic cost of the heat exchanger is given in terms of the following heat transfer area:

$$\log \dot{C}_{HX} = K_{1,HX} + K_{2,HX} (\log A_{HX}) + K_{3,HX} (\log A_{HX})^2. \tag{25}$$

$K_{1,HX}$ ,  $K_{2,HX}$ , and  $K_{3,HX}$  are the constants for the type of heat exchanger. The pressure factor is given by the following:

$$\log F_{PHX} = C_{1,HX} + C_{2,HX} (\log P_{HX}) + C_{3,HX} (\log P_{HX})^2. \tag{26}$$

$C_{1,HX}$ ,  $C_{2,HX}$ , and  $C_{3,HX}$  are the constants for the heat exchanger type. The total cost of the pump is obtained as follows:

$$C_{PP} = \frac{527.7}{397} F_S \dot{C}_{PP} \left\{ B_{1,PP} + (B_{2,PP} F_{M,PP} F_{P,PP}) \right\}. \tag{27}$$

$B_{1,PP}$  and  $B_{2,PP}$  are the constants for the pump type,  $F_{M,PP}$  is the additional material factor,  $F_{P,PP}$  is the pressure factor for the pump, and  $\dot{C}_{HX}$  is the basic cost of the pump. The basic cost of the pump is given in terms of pump power:

$$\log \dot{C}_{PP} = K_{1,PP} + K_{2,PP} (\log W_{PP}) + K_{3,PP} (\log W_{PP})^2. \tag{28}$$

$K_{1,PP}$ ,  $K_{2,PP}$ , and  $K_{3,PP}$  are the constants for the pump type. The pressure factor for the pump is calculated as follows:

$$\log F_{P,PP} = C_{1,PP} + C_{2,PP} (\log P_{PP}) + C_{3,PP} (\log P_{PP})^2. \tag{29}$$

$C_{1,PP}$ ,  $C_{2,PP}$ , and  $C_{3,PP}$  are the constants for the pump type. The cost of the turbine is given by the following:

$$C_{TR} = \frac{527.7}{397} \times F_S \times \dot{C}_{TR} \times F_{M,TR}. \tag{30}$$

$F_{M,TR}$  is the pressure and material factor for the turbine, and  $\dot{C}_{TR}$  is the basic cost of the turbine.

$$\log \dot{C}_{TR} = K_{1,TR} + K_{2,TR} (\log W_{TR}) + K_{3,TR} (\log W_{TR})^2. \tag{31}$$

Table 4. Constants for economic modeling.

Cont.	Value	Cont.	Value	Cont.	Value
$F_S$	1.700	$K_{2,HX}$	-0.1557	$B_{1,PP}$	1.890
$B_{1,HX}$	0.960	$K_{3,HX}$	0.1547	$B_{2,PP}$	1.350
$B_{2,HX}$	1.210	$C_{1,HX}$	0.0000	$F_{M,PP}$	2.200
$F_{M,HX}$	2.400	$C_{2,HX}$	0.0000	$K_{1,PP}$	3.389
$K_{1,HX}$	4.660	$C_{3,HX}$	0.0000	$K_{2,PP}$	0.536
$F_{M,TR}$	3.500	$C_{2,PP}$	0.3957	$K_{3,PP}$	0.153
$K_{1,TR}$	2.265	$C_{3,PP}$	-0.0022	$C_{1,PP}$	-0.393
$K_{2,TR}$	1.439	$K_{3,TR}$	-0.1776	$K_{3,TR}$	-0.177

$K_{1,TR}$ ,  $K_{2,TR}$ , and  $K_{3,TR}$  are the constants for the turbine type. The specific investment cost is calculated by the following relation:

$$Specific\ Investment\ Cost(SIC) = \frac{W_t - W_p}{TC} \quad (32)$$

The constants for the economic modeling of the ORC system are shown in Table 4.

### 3.4 Greenhouse gas emission

The emission from the fossil fuel power plant was estimated using the fuel analysis approach [20]. Three different fossil fuel power generation systems were investigated: coal, natural gas, and diesel oil. The GHGs associated with the burning of fossil fuel are mainly CO<sub>2</sub>, CH<sub>4</sub>, and N<sub>2</sub>O. CO<sub>2</sub> is the major contribution of GHG emission from fossil fuel. Thus, the effect of CH<sub>4</sub> and N<sub>2</sub>O is calculated relative to CO<sub>2</sub>. The fuel analysis approach is adopted to calculate the CO<sub>2</sub> emission as follows:

$$CO_2(kg) = \sum_i^n (m_f)_i \cdot HC_i \cdot C_i \cdot FO_i \cdot \left[ \frac{(CO_2)_{m.w}}{(C)_{m.w}} \right], \quad (33)$$

where  $HC_i$  is the heat content,  $C_i$  is the carbon content,  $FO_i$  is the fraction of oxidized fuel, and  $m.w$  is the molecular weight. The CH<sub>4</sub> and N<sub>2</sub>O emissions are calculated by the following:

$$\begin{aligned} CH_4\ Emission(kg) &= A_S \times EF_S \\ N_2O\ Emission(kg) &= A_S \times EF_S \end{aligned} \quad (34)$$

where  $A_S$  is the activity level of a specific source category, and  $EF_S$  is the emission factor of that category. The CH<sub>4</sub> and N<sub>2</sub>O emissions depend on fuel type, combustion technology, combustion characteristics, and control technologies.

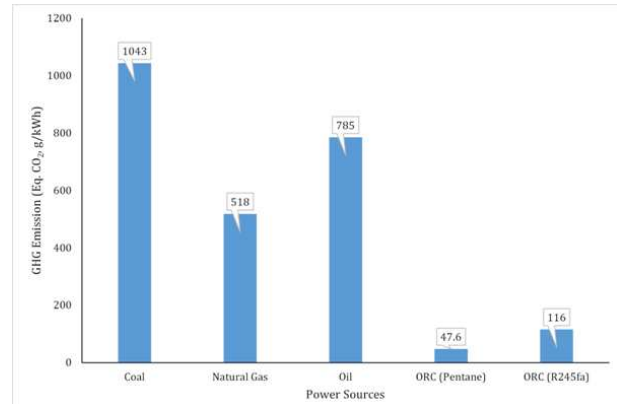


Fig. 4. Equivalent CO<sub>2</sub> emission from different power sources.

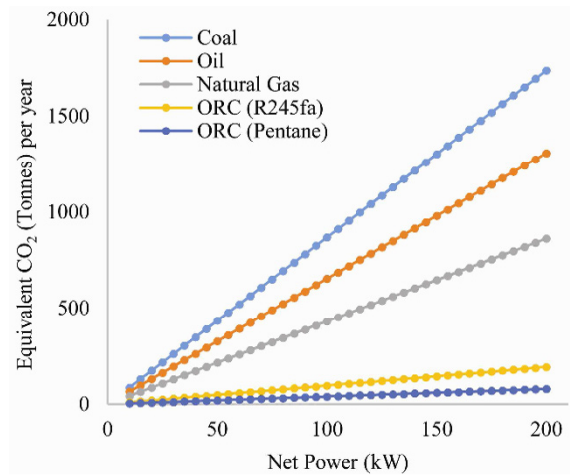


Fig. 5. Greenhouse gas emission variation with net power.

The environmental protection agency provides the basic guidelines for estimating the activity level based on fuel type, fuel combustion technology and characteristics, control technologies, and specific application.

### 4. Results and discussion

The GHG emission of ORC plants is less than that of conventional fossil fuel power plants because no combustion is involved in the former. The equivalent CO<sub>2</sub> for the ORC and fossil fuel power sources are shown in Fig. 4.

Coal has the highest emission, and ORC has the lowest emission value of equivalent CO<sub>2</sub>. The selected working fluid affects the CO<sub>2</sub> emission to some extent, but it is negligible compared with fossil fuel power sources.

GHG emission is directly related to the power produced and the annual equivalent CO<sub>2</sub> from 10 kW to 200 kW for fossil fuel; ORC is shown in Fig. 5. At a small power capacity, the difference in the GHG emissions of ORC and fossil fuel is negligible. After 50 kW, the difference increases rapidly. In the current scenario, the net power of R245fa and pentane was calculated under the considered conditions.

The amount of GHG emission that can be reduced per an-

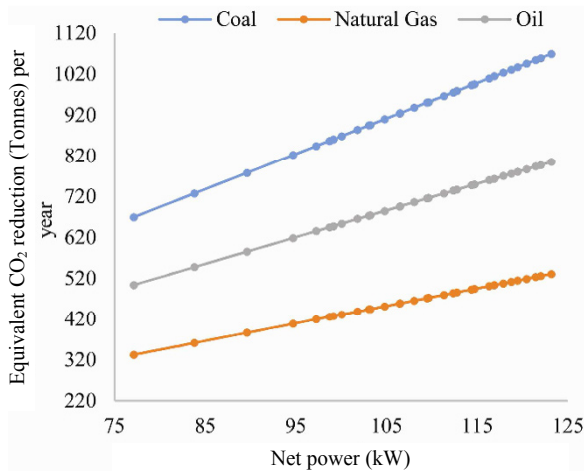


Fig. 6. Greenhouse gas reduction by ORC (R245fa).

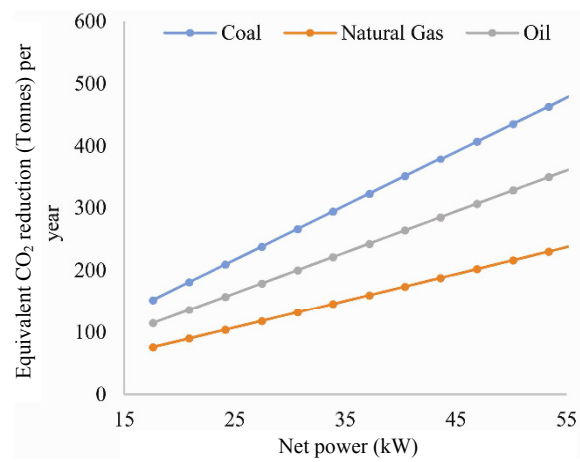


Fig. 7. Greenhouse gas reduction by ORC (pentane).

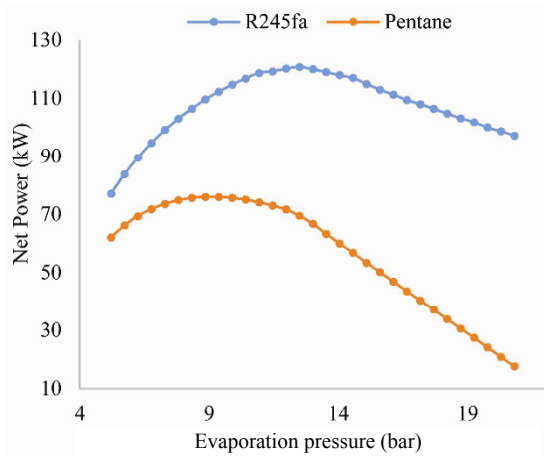


Fig. 8. Effect of evaporation pressure over the net power of ORC.

num by this power, taking the equivalent power of fossil fuels as base, is shown in Figs. 6 and 7.

The GHG emission reduction of the R245fa-based ORC system is much higher than that of the pentane-based ORC system. The net power produced by the two working fluids at

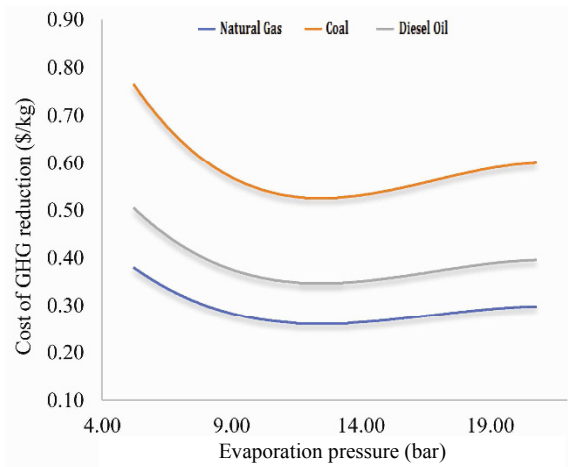


Fig. 9. Greenhouse gas reduction cost for ORC (R245fa).

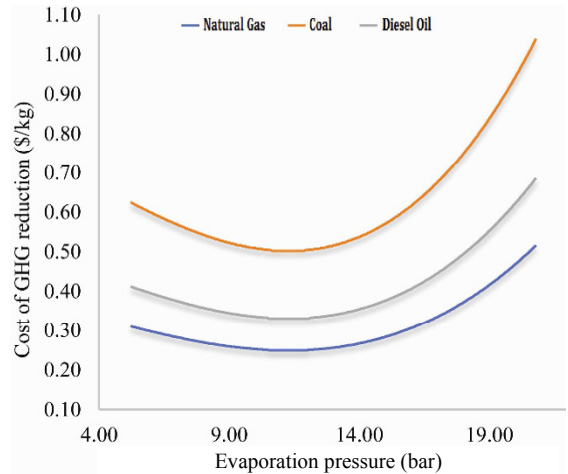


Fig. 10. Greenhouse gas reduction cost for ORC (pentane).

the same operating condition is different. Therefore, the GHG emission reduction potential of both working fluids is also different.

The variation in the power produced by R245fa and pentane over a range of evaporation pressure is shown in Fig. 8. The optimum evaporation pressure for both working fluids is different. For example, the saturation temperature of R245fa at 10 bar is 89.74°C, whereas the saturation pressure of pentane at 10 bar is 124°C.

Therefore, the mass flow rate of pentane is reduced, thereby resulting in a low net power. The economics of the ORC system for GHG reduction are shown in Figs. 9 and 10. The economic assessment was performed by dividing the total investment cost of the ORC system by the net GHG emission per year. The fossil fuel-based GHG emission was used as the reference for comparing the reduction cost for R245fa and pentane.

The reduction cost of GHG for R245fa is lower than 0.8 \$/kg. It was initially higher because of the low net power output of ORC at low evaporation pressure and was minimum at 10 bar, after which it increased. The reduction of GHG cost



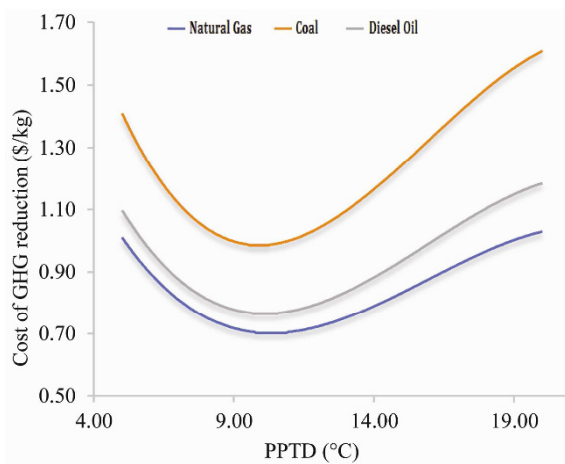


Fig. 11. Greenhouse gas reduction cost and PPTD.

was followed by the net power output of the ORC system. A similar trend was observed for pentane, which showed a relatively high GHG reduction cost because of its low net power.

The pinch point temperature difference (PPTD) is one of major factors that strongly affect the ORC net power and economics. The effect of PPTD on GHG reduction is shown in Fig. 11. The GHG reduction cost for each fossil fuel plant initially decreased and then increased. As the pinch point temperature increased, the net power decreased because the evaporation pressure was lowered, and consequently the cost decreased.

From 5°C to 10°C, the decrease in the net power was compensated for by the cost. The specific investment cost of ORC (\$/kW) decreased, which in turn decreased the GHG emission reduction cost. From 5°C to 10°C, the decrease in the net power was compensated for by the cost. The specific investment cost of ORC (\$/kW) decreased, which in turn decreased the GHG emission reduction cost. A further increase in the pinch point temperature beyond 10°C rapidly increased the specific investment cost because of the decrease in net power. A low net power results in low evaporation pressure.

## 5. Conclusion

The ORC system can be used to recover low-grade waste heat, thereby ultimately reducing the GHG emission and increasing the efficiency of the primary system. The GHG reduction potential of ORC strongly depends on its operating conditions and working fluid. The GHG reduction potential of ORC with R245fa is higher than that with pentane because of the high net power of the former under the same operating conditions. The cost of GHG reduction through the ORC system with R245fa is less than 0.4 \$/kg to 0.8 \$/kg based on the fossil fuel used for alternate power. By contrast, the GHG reduction cost through the ORC system with pentane is 0.4 \$/kg to 1 \$/kg, which is based on the annual GHG reduction potential through ORC. ORC incurs no operating cost; thus, the cost is low if the ORC system operates for more than one

year. For a 20-year life cycle of an ORC plant, the cost is further reduced to 0.02 \$/kg to 0.04 \$/kg for R245fa and 0.04 \$/kg to 0.05 \$/kg for pentane. The reduction cost depends on the operating condition of the ORC system, particularly its evaporation pressure. The pinch point in the evaporator and condenser affects the cost of ORC and net power and directly affects the GHG reduction potential and economics.

## Acknowledgment

This work was conducted under the framework of the research and development program of the Korea Institute of Energy Research (B4-2461).

## References

- [1] B. F. Tchanche, Gr. Lambrinos, A. Frangoudakis and G. Papadakis, Low-grade heat conversion into power using organic Rankine cycles – A review of various applications, *Renewable and Sustainable Energy Reviews*, 15 (8) (2011) 3963-3979.
- [2] V. H. Maria, *CO<sub>2</sub> Emissions from fuel combustion highlights*, International Energy Agency (2012).
- [3] BCS, Incorporated, *Waste heat recovery: Technology and opportunities in U.S. industry*, U.S. Department of Energy (2008).
- [4] M. A. Khatita, T. S. Ahmed, F. H. Ashour and I. M. Ismail, Power generation using waste heat recovery by organic Rankine cycle in oil and gas sector in Egypt: A case study, *Energy*, 64 (1) (2014) 462-472.
- [5] D. Wang, X. Ling and H. Peng, Performance analysis of double organic Rankine cycle for discontinuous low temperature waste heat recovery, *Applied Thermal Engineering*, 48 (15) (2012) 63-71.
- [6] F. A. Al-Sulaiman, I. Dincer and F. Hamdullahpur, Exergy analysis of an integrated solid oxide fuel cell and organic Rankine cycle for cooling, heating and power production, *Journal of Power Sources*, 195 (8) 15 (2010) 2346-2354.
- [7] K. Tom, *Combined heat and power: evaluating the benefits of greater global investment*, International Energy Agency (2008).
- [8] K. Tom, *Combined heating and power and emissions trading: options for policy makers*, International Energy Agency (2008).
- [9] O. Balli, H. Aras and A. Hepbasli, Thermodynamic and thermoeconomic analyses of a trigeneration (TRIGEN) system with a gas-diesel engine: Part II – An application, *Energy Conversion and Management*, 51 (11) (2010) 2260-2271.
- [10] X. Q. Kong, R. Z. Wang and X. H. Huang, Energy efficiency and economic feasibility of CCHP driven by stirling engine, *Energy Conversion and Management*, 45 (9-10) (2004) 1433-1442.
- [11] P. Ahmadi, I. Dincer and M. A. Rosen, Exergo-environmental analysis of an integrated organic Rankine cy-



- cle for trigeneration, *Energy Conversion and Management*, 64 (2012) 447-453.
- [12] P. Ahmadi and I. Dincer, Exergoenvironmental analysis and optimization of a cogeneration plant system using Multimodal Genetic Algorithm (MGA), *Energy*, 35 (12) (2010) 5161-5172.
- [13] C. Liu, C. He, H. Gao, H. Xie, Y. Li, S. Wu and J. Xu, The environmental impact of organic Rankine cycle for waste heat recovery through life-cycle assessment, *Energy*, 56 (1) (2013) 144-154.
- [14] M. Li, J. Wang, S. Li, X. Wang, W. He and Y. Dai, Thermo-economic analysis and comparison of a CO<sub>2</sub> transcritical power cycle and an organic Rankine cycle, *Geothermics*, 50 (2014) 101-111.
- [15] M. Imran, B. S. Park, H. J. Kim, D. H. Lee, M. Usman and M. Heo, Thermo-economic optimization of regenerative organic rankine cycle for waste heat recovery applications, *Energy Conversion and Management*, 87 (2014) 107-118.
- [16] B. Thonon, *Design method for plate evaporators and condensers*, 1st International Conference on Process Intensification for the Chemical Industry, BHR Group Conference Series Publication, 18 (1995) 37-47.
- [17] Y. Y. Hsieh and T. F. Lin, Saturated flow boiling heat transfer and pressure drop of refrigerant R-410A in a vertical plate heat exchanger, *International Journal of Heat and Mass Transfer*, 45 (5) (2002) 1033-1044.
- [18] D.-H. Han, K.-J. Lee and Y.-H. Kim, Experiments on the characteristics of evaporation of R410A in brazed plate heat exchangers with different geometric configurations, *Applied Thermal Engineering*, 23 (10) July (2003) 1209-1225.
- [19] D.-H. Han, K.-J. Lee and Y.-H. Kim, The characteristics of condensation in brazed plate heat exchangers with different chevron angles, *Journal of the Korean Physical Society*, 43 (1) (2003) 66-73.
- [20] Direct Emissions from Stationary Combustion Sources, United States Environmental Protection Agency (EPA), May (2008).



**Muhammad Imran** is a Ph.D. student of Energy System Engineering at the University of Science and Technology, Daejeon, Korea. His research interests include thermodynamic analysis and optimization for sustainable energy systems. The investigation of heat transfer and pressure drop characteristics of the organic Rankine cycle working fluids in heat exchangers is one of the core research areas of his Ph.D. works.



**Byung-Sik Park** is a principal researcher at the Korea Institute of Energy Research, Korea. He received his doctorate degree from Chungnam National University, Daejeon, Korea. He has over 20 years of experience in research and development of national projects, focused on district heating, organic Rankine cycle systems, Stirling engines, and combined heat and power systems.



**Hyouck-ju Kim** is a principal researcher at the Korea Institute of Energy Research, Korea. He received his doctorate degree from Kyungpook National University, Daegu, Korea. His research interests include district heating, Stirling engines, design and optimization of CHP systems, and combustion engineering.